Co/Ni/Al-LTH layered triple hydroxides with zeolitic imidazolate frameworks (ZIF-8) as high efficient removal of diazinon from aqueous solution

Abdolraouf Samadi-Maybodi (samadi@umz.ac.ir)
https://orcid.org/0000-0001-6334-567X
Hashem Ghezel-Sofla

Research Article

Keywords: Diazinon, Removal of pollutants, Layered triple hydroxide, BOX-Behnken design, Response surface methodology

Posted Date: April 21st, 2022

DOI: https://doi.org/10.21203/rs.3.rs-1562659/v1

Abstract

Today, high consumption and increasing use of pesticides and chemical fertilizers to control pests of agricultural products, and the entry of these pollutants into the environment, is one of the most important environmental and health problems. Their non-biodegradability, as well as their toxicity and carcinogenicity, have generally made these compounds one of the most dangerous pollutants that cause inevitable pollution of the environmental.

Among the various methods used to remove agricultural pesticide residues from the water sources, the adsorption method has received more attention due to its simplicity, cost and higher efficiency.

In this research, nanocomposite of Co/Ni/Al-LTH@ZIF-8 was synthesized by *in-situ* growth of ZIF-8 on the Co/Ni/Al-LTH and used for the removal of diazinon pesticide from aqueous solution. Characterizations of the nanocomposite were performed by various techniques, including Fourier transform infrared spectroscopy, X-ray diffraction, field emission scanning electron microscopy, energy dispersive X-ray spectroscopy and thermal analysis. Statistical evaluation was studied by BOX-Behnken design. In addition, the response surface methodology was used to optimize the factors affecting on the adsorption process. Parameters such as adsorbent dose (mg), pH, and contact time (min) were considered in this experiment. Results revealed that the removal efficiency of diazinon was significantly improve (from 64% to 84%) by loading ZIF-8 on the Co/Ni/Al-LTH. Statistical studies showed the optimum conditions achieved under pH=6.9, adsorbent dosage 25 mg, and contact time 12 min.

1. Introduction

Crop production are essential for human nutrition. The Food and Agriculture Organization of the United Nations (FAO) defines food security as food availability, food access, and food usage. However, in order to rapid increase in food production, annually thousands tons of pesticides are used in the world [1]. Pesticides pollutions are considered an important concern in the world because many of such compounds are dangerous to both human health and the environment. Agricultural pesticides are one of the major pollutants, and this has raised concerns regarding the protection of health and the environment and hence must be controlled to minimize contamination problems. [2, 3]. Different types of pesticides such as organophosphorus and organochlorine are used in agriculture [4]. Organophosphate pesticide is one of an important category of pesticides that are mostly used in agriculture. Among organophosphorus pesticides, diazinon is widely used in agricultural for the struggle against pests. Diazinon is a kind of organophosphate pesticide. It is utilized as a control measure for pests in fruits, vegetables and field crops, but excessive consuming of this insecticide leads to contaminate the environment and consequently removal of this compound is essential concern. The LD50 for diazinon in male and female Rat oral are 1340 and 1160 mg/kg [5]. The presence of such poisons causes to interact with enzyme of acetyl cholinesterase and consequently leads to neurological disorders [6]. The solubility of diazinon in water is low, as a result, they remain in the soil for a long time and cause surface water and groundwater pollution [7].

Several techniques were employed to remove pesticides from water and wastewater by the various methods, for instance electrochemical [8] photocatalytic degradation [9] biodegradation [10] and adsorption [11].

The absorption method is more common and applicable due to its design, readily available, simplicity, low cost, and higher efficiency. Removal of pesticides from aqueous solutions is performed by the various adsorbent, such as, activated carbon [12] carbon nanotubes [13] graphene oxide [14] zeolites [15] and metal organic framework (MOF) [16] are used to remove pesticides from aqueous solutions.

Layered double hydroxides (LDHs), have received a great attention in various fields of chemistry in recent years. An LDH is represented by the general formula $[M^{2+}_{1-x}M^{3+}_{x}(OH)_2]^{x+}(A^{n-})_{x/n}\cdot mH_2O$, where M^{2+} and M^{3+} are divalent and trivalent metals cations and A^{n-} is the interlayer anion [17]. Due to the unique molecular structure of LDHs, they exhibit desirable chemical and physical properties, such as high surface area, catalytic ability, anion exchange capability, high mechanical and thermal stability and tunable of interlayer spaces [18]. LDHs are widely used in adsorption process for removal of contaminant from water. The distance between the layers of LDHs are adjustable with access to the guest anions through the process of chemical synthesis. Therefore, these materials have led to a promising approach for removal of organic contaminants from wastewater and water purification. However, The LDH has some disadvantages such as porosity and relatively low surface area [19]. Porous materials such as metal organic frameworks (MOFs) are great interest to overcome this impediment for removal processing.

Zeolitic imidazolate frameworks (ZIFs) represent a unique class of (MOFs) in which the network topology and related properties vary greatly while core chemical connectivity is retained [20]. ZIFs are composed of tetrahedrally-coordinated transition metal ions (e.g. Fe, Co, Cu, Zn) connected by imidazolate linkers [21]. ZIFs have a higher surface area than zeolites and they are more thermally and chemically stable than other MOFs [22]. As a result, these features, select ZIFs suitable for use in the field of adsorption [23].

In this work, ZIF and layered triple hydroxide (LTH) was successfully synthesized via a facile one-step in situ hydrothermal method. The as-synthesized Co/Ni/Al- LTH@ZIF-8 hybrids were characterized by SEM, EDS, XRD, FT-IR, TGA, BET and Zeta potential methods. Subsequently as-synthesized Co/Ni/Al- LTH@ZIF-8 nanocomposites were applied for the removal of diazinon pesticide from the aqueous solutions. Various factors influencing on the adsorption process including the adsorbent dosage, the pH of the solution, and contact time were investigated in detail. The Box–Behnken design was performed for optmization.

2. Experimental

2.1. Reagents and Chemicals

The chemical substances of $CoCl_2.6H_2O$, $NiCl_2.6H_2O$, $AlCl_3.9H_2O$, NaOH (99%), ethanol (96%), $Zn(NO_3)_2.6H_2O$, 2-methylimidazole, methanol (99.8%), H_2SO_4, HNO_3 and diazinon were purchased from Merck Company. All chemicals compounds were used without further purification.

Stock solution of diazinon (1000 mg/L) was prepared in mixture of methanol and water (50/50 by volume) and kept in a refrigerator at -18°C until use.

2.2. Instrument and software

X-ray diffraction (XRD) patterns were recorded by an X-ray diffractometer (PHILIPS-PW1730) using Cu K_α radiation (1.5 Aº) in the range of 2θ 0.8º to 70º with a scanning rate of 0.05 degree/second. Field emission scanning electron microscopy coupled with energy dispersive X-ray spectrometer (FESEM/EDX) model TESCAN-MIRA III. (BELSORP MINI 2) was used to obtain the morphology of the synthesized samples. The FT-IR spectra of the prepared samples were recorded by Thermo/FT-IR AVATAR spectrophotometer in the range of 600–4000 cm^{-1} at room temperature. The porosity and surface area of the samples was studied by the Brunauer–Emmet–Teller (BET) method using nitrogen adsorption/desorption isotherms at 77 K on a BELSORP MINI II device. Electronic absorbance spectra were recorded using a UV–vis spectrophotometer (PG Instrument Ltd, double beam-Model T90+) with spectral range of 190–350 nm. In order to find of the optimized conditions of the removal efficiency of diazinon by Co/Ni/Al-LTH@ZIF the Box-Behnken design method was performed (Design Expert software,version 7, State-Ease, Inc., United States).

The response surface methodology (RSM) and BBD method was implemented to optimize the effect of different factors of the removal efficiency of diazinon by Co/Ni/Al-LTH@ZIF. (Design Expert software, version 13, State-Ease, Inc., 3 United States). Energy dispersive Xray (EDX) spectra were recorded on an EDX Genesis XM2 attached to SEM. The zeta potential of nanoparticles was measured by Horiba (SZ-100) at room temperature.

2.3. Synthesis of layer triple hydroxide (Co/Ni/Al-LTH)

Conventional hydrothermal method was used to synthesize Co/Ni/Al-LTH adsorbent with a molar ration of $Co^{2+}/Ni^{2+}/Al^{3+}$=2:2:4. In a typical experiment, 80 mmol $CoCl_2.6H_2O$, 80 mmol $NiCl_2.6H_2O$ and 40 mmol $AlCl_3.9H_2O$ were dissolved in 30 mL deionized water. Subsequently, 50 mL of 3 M NaOH solution was added dropwise to the above solution under vigorous magnetic stirring at room temperature (22 ± 1 °C). The pH of the reaction solution was adjusted 12. The resultant mixture was transformed into a 100 mL Teflon-lind stainless steel autoclave and followed by heated at 180 ºC for 24h. After cooling to room temperature, the insoluble solids were separated by filtration and washed with distilled water and ethanol, then kept in oven at 80°C for overnight.

2.4. Synthesis of ZIF-8 nanocrystals

ZIF-8 nanocrystals were synthesized with Zn^{2+}: 2-methylimidazole: methanol molar ratio of 1: 80: 4000 according to the route reported previously with some modifications [24]. For this propose, two separate

solutions were prepared as follows; solution A: 6 g of $Zn(NO_3)_2$ was dissolved in 100 mL methanol; solution B: 16 g of 2-methylimidazole was dissolved in 100 mL methanol. Then solutions A and B were mixed under vigorous agitation until the mixture turned cloudy. After 6 h, precipitate were collected by centrifuging (8500 rpm, 20 min), then washed with methanol for three times. Finally, the white product (ZIF-8) was dried overnight at 80 °C.

2.5. Synthesis of LTH@ZIF-8 composite

12 g of $Zn(NO_3)_2.6H_2O$ was dissolved in 50 mL methanol and gradually added in to a dispersed solution of Co/Ni/Al-LTH (0.2 g in 10 mL methanol). Then 2-methylimidazole solution (4.5 g in 50 mL of methanol) was added to the above solution under vigorous magnetic stirring at room temperature for 4 h. The light brown precipitate was collected by centrifuging (8500 rpm, 20 min) and washed several times with water and ethanol, respectively and dried in oven at 80 ºC for overnight.

2.6. Measurement of diazinon uptake

Standard solutions of diazinon with different concentrations (5 to 50 ppm) were prepared by dilution of its stock solution (1000 ppm). Due to the low solubility of diazinon in water, all solutions were prepared using mixture of methanol and water (50/50 volume ratio). Calibration curve was constructed by plotting absorption (A) against concentration of the standard solutions. Absorption of the solutions was measured by UV–vis spectrophotometry at maximum wavelength (λ_{max}) 247 nm. The removal percentage was calculated according to following equation.

$$Removal(\%) = \frac{\left(C_0 - Ce\right)}{C_0} \times 100$$

1

where C_o and C_e are initial and equilibrium concentrations (mg L^{-1}), respectively.

The adsorption capacity (q_t) of the adsorbents was calculated by Eq. 2.

$$q_t = \frac{\left(C_0 - Ce\right)V}{W}$$

2

where, V is the volume (L) of the solution and W is the mass (g) of the adsorbent [25].

3. Results And Discussion

3.1. Characterization of synthesized nanocomposites

The synthesized samples were characterized with several techniques as follows:

3.1.1- XRD patterns

Figure 1 (a–c) illustrates the XRD patterns of Co/Ni/Al-LTH, ZIF-8 and LTH@ZIF-8 nanoparticles respectively. In Fig. 1a, the sharp diffraction peaks positioned at 2θ = 11.80°, 19.50°, 23.20°, 38.95°, 52.40°, 59.60°, 61.30° and 62.60° associated with the Miller indices of (003), (006), (009), (018), (110), (113), (012) and (015) respectively represent the crystallographic structure of Co/Ni/Al-LTH. The peaks at 11.80°, 19.50° and 23.20° ascribed to Miller indices of (003), (006), and (009) indicate the stacking order of layers in LTH [26].

Figure 1b displays the XRD pattern of ZIF-8 peaks located at 2θ = 6.55°, 10.47°, 12.60°, 14.50°, 16.30°, 17.90°, 22.05°, 24.45°, 25.55°, 26.50°, 27.65°, 28.90°, 29.55°, 30.55°, 31.35°, 32.25°, 34.85° and 36.35° are associated with the Miller indices of (011), (002), (112), (022), (013), (222), (114), (233) and (224), respectively. By considering and comparison this result with the previous reports [27, 28] it can be said, this compound was well synthesized. Figure 1c exhibits the XRD pattern of the Co/Ni/Al-LTH @ZIF-8 nanocomposite, as can be observed this pattern almost consists of both peaks in XRD patterns of Co/Ni/Al-LTH and ZIF-8. Results reveal that the combination of Co/Ni/Al-LTH and ZIF-8 nanomaterials does not disturb their regular structure and the nanocomposite was successfully synthesized.

3.1.2. Studies of FT-IR

Figure 2(a-c) illustrates FT-IR spectra of Co/Ni/Al-LTH, ZIF-8 and Co/Ni/Al-LTH/ZIF-8 composite. Figure 2a shows the FT-IR spectrum of the Co/Ni/Al-LTH. The narrow peak at 3636 cm^{-1} can be attributed to the non-hydrogen-bonded hydroxyl groups. the broad peak around 3568 cm^{-1} can be assigned to the O–H stretching modes of the interlayer water molecules and the H-bound O–H groups and the peak at 1714 cm^{-1} is attributed to the bending mode vibration of the interlayer water molecule. The absorption around 1419 cm^{-1} can be assigned to the intercalated carbonate anions [29]. Absorption bands observed in 1093, 1223 and 1363 cm^{-1} can be ascribed to interlayer nitrate groups [30]. Absorption bands around 1000 cm^{-1} are due to the stretching and bending vibrations modes of M-O and M-OH. (M = Co^{2+}, Ni^{2+}, Al^{3+})

Figure 2b shows the FT-IR spectrum of the ZIF-8 metal organic network. The bands observed at 689 and 755 cm^{-1} can be ascribed to the stretching vibrations modes of the Zn-N and Zn-O bonds, respectively [31]. Also, the bands related to 1143 ,1584 and 2927 cm^{-1} can be associated to the C-N, C = N and C-H stretching vibrations modes in the imidazole ring, respectively. Figure 2c exhibits the FT-IR spectrum of the Co/Ni/Al-LTH@ZIF-8 nanocomposite as can be observed this spectrum almost includes of both signals in spectra of (2a) and (2b).

3.1.3. Morphology studies of the synthesized samples

The surface morphology of the Co/Ni/Al-LTH@ZIF-8 was examined by field emission scanning electron microscopy. Figures 3a -3c illustrate FESEM images of the Co/Ni/Al-LTH, ZIF-8 and Co/Ni/Al-LTH @ ZIF-8,

respectively and Figs. 3d and 3e show the EDX spectra of the ZIF-8 and Co/Ni/Al-LTH @ ZIF-8. Figure (a) shows the images of Co/Ni/Al-LTH nanosheets as hexagonal nanoplates with a size of about 100–200 nm. Figure 3 (b) shows images of ZIF-8 particles with a uniform polygonal structure measuring approximately 30–60 nm. Figure 3 (c) exhibits the FESEM images of the Co/Ni/Al-LTH @ ZIF-8 composite. The morphology of Co/Ni/Al-LTH @ ZIF-8, has a moderately change with the Co/Ni/Al-LTH images, transforming from hexagonal nanoplates to spherical shape (Fig. 5a & b). The EDX spectra with the tables of elemental composition of EDX confirm that ZIF-8 and Co/Ni/Al-LTH @ ZIF-8 composite are presented in Fig. 3 (d,e). Results of EDX confirm that the Co/Ni/Al-LTH @ ZIF-8 nanohybrid was successfully synthesized.

3.1.4. Thermal analysis

Results of thermal analysis of Co/Ni/Al-LTH, ZIF-8 and Co/Ni/Al-LTH/ZIF-8 are presented in Fig. 4(a-c). Figure 4(a) shows thermogram of Co/Ni/Al-LTH that contains two steps. In the first step, due to the evaporation of water molecules present on the surface and as well as interlayer water molecules, within the range of 50–280°C temperature. In the second step, weight loss observed at a temperature range of 280–350°C is ascribed the dehydroxylation of the brucite-like metal layers and the release of intercalated anions [32].

Figure 4(b) presents the thermogram of ZIF-8, a graduate weight loss owing to evaporation of water molecules absorbed on the surface and in cavities of the compound below 200°C. The second weight-loss stage belongs to decomposition of the organic ligand 2-methylimidazole. Eventually, degradation of the metal organic framework is the reason for the weight loss of the third stage [33]. Figure 4c shows thermal behavior of the Co/Ni/Al-LTH@ZIF-8 composite. The weight loss of the first and second stages related to solvent extraction and dehydroxylation in Co/Ni/Al-LTH nanoparticles and the third stage is related to the decomposition of the ZIF-8 metal organic framework in the Co/Ni/Al-LTH@ZIF-8 composite.

Figure 5 shows the surface charge evaluation of the adsorbents synthesized in this study through the zeta potential. The zero-point charge (zpc) of nanocomposit particles is around 10. This value is very close to the zpc of the ZIF-8 [34]. This pronounces that Co/Ni/Al-LTH is covered by ZIF-8 particles and reconfirming above results. The adsorbent surface will be negatively charged surfaces when pH > pzc and in contrast will be positively charged when pH < pzc. Hence the adsorption process is influenced by the repulsion or attraction forces between adsorbent and adsorbate, this phenomenon due to the pzc of the adsorbent (i.e., Co/Ni/Al-LTH /ZIF-8) and pK_a of the adsorbate (i.e., diazinon) and also pH of the solution. As a result, to find higher removal efficiency, the pH value of the solution would be optimized.

3.1.5. Adsorption isotherm studies

Figure 6 *(a-c) shows the Nitrogen adsorption/desorption (BET method) and pore size distribution curves (BJH method) of Co/Ni/Al-LTH, ZIF-8 nanoparticles and Co/Ni/Al-LTH@ZIF-8 composite, respectively. According to the IUPAC classification, the synthesized Co/Ni/Al-LTH can be categorized as type IV with H4 hysteresis loop (*Fig. 6a*), which indicates the existence of slit-like mesoporous structures of the corresponding compound* [37]. *As shown in* Fig. 6b, *the ZIF-8 nanoparticle isotherm represents type I,*

which is characteristic of microporous materials. Figure 6c *is similar to the* Fig. 6b *indicate that the nanohybride of Co/Ni/Al-LTH@ZIF consists microspore, and also its isotherm is classified as type I.*

Table 1 *presents the total surface area (S_{BET}) and total pore volume for the synthesized LTH, ZIF-8 and nanocomposites, respectively. Both surface area and total pore volume of Co/Ni/Al-LTH@ZIF is very close to the ZIF-8, nevertheless both aforementioned parameters are significantly more than that for Co/Ni/Al-LTH.*

Table 1
BET results of the synthesized samples.

Adsorbent	*S_{BET} (m^2g^{-1})*	*Total pore volume (cm^3g^{-1})*	*Mean pore diameter (nm)*
Co/Ni/Al-LTH	*28.8*	*0.027*	*3.8*
ZIF-8	*1370*	*0.523*	*1.52*
Co/Ni/Al-LTH@ZIF	*1030*	*0.401*	*1.54*

3.2. Design expert and optimization

An experimental design method was planned using Design Expert 13 software in which the surface response design technique is employed based on the Box–Behnken method. The parameters of adsorbent dose, pH, and contact time were selected as the main affecting factors for removal of diazinon. Table 2 shows three levels (low (1−), medium (0), and high (+ 1)).. Table 3shows the Box-Behnken design matrix by considering three factor-three levels of input parameters and the corresponding output response for the removal of diazinon by the Co/Ni/Al-LTH /ZIF-8.

Table 2
Experimental range and level of factors in Box-Behenken Design.

Factors	**Levels**		
	(-1)	(0)	(+ 1)
Adsorbent dose (mg)	10	20	30
pH	4	7	10
Contact time (min)	10	20	30

Table 3
Box-Behenken design matrix for three factors along with observed predicted responses.

Run	Adsorbent dose (A)	pH (B)	Contact time (C)	Removal of DIZ (%)
1	10	10	20	60.76
2	20	4	10	64.27
3	10	7	30	71.29
4	20	7	20	82.69
5	20	7	20	82.61
6	30	4	20	68.65
7	20	7	20	81.71
8	20	10	10	73.04
9	20	7	20	82.69
10	10	7	10	71.29
11	30	10	20	69.53
12	20	7	20	81.82
13	30	7	10	83.57
14	10	4	20	53.74
15	20	10	30	67.8
16	20	4	30	67.67
17	30	7	30	83.98

In this study, results of the analysis of variance (ANOVA) were performed using Design Expert 13 software. In accordance with the conventional acceptance of statistical significance, at a 95% confidence level, the p-value must be less than 0.05 to be meaningful. If the p value for non-compliance is greater than the value selected for significance at a confidence level, it indicates that the model is desirable [35].

According to the p values obtained from the results of ANOVA (Table 4), all three factors considered in the removal of diazinon was significance.

Table 4
Result of analysis of variance (ANOVA)

Source	Sum of Squares	df	Mean Square	F-value	p-value	
Model	1351.19	9	150.13	540.45	< 0.0001	significant
A	295.85	1	295.85	1065.02	< 0.0001	
B	35.28	1	35.28	127.00	< 0.0001	
C	0.2556	1	0.2556	0.9202	0.3694	
AB	9.42	1	9.42	33.93	0.0006	
AC	0.0420	1	0.0420	0.1513	0.7089	
BC	18.66	1	18.66	67.18	< 0.0001	
A^2	101.02	1	101.02	363.66	< 0.0001	
B^2	853.29	1	853.29	3071.69	< 0.0001	
C^2	0.0676	1	0.0676	0.2435	0.6368	
Residual	1.94	7	0.2778			
Lack of Fit	0.9658	3	0.3219	1.32	0.3857	not significant
Pure Error	0.9787	4	0.2447			
Cor Total	1353.13	16				
Adjusted R^2=0.9967, R^2=0.9986, Predicted R^2=0.9874, Adequate Precision = 74.7984						
• A = Adsorbent dose B = pH C = Contact time						

Figure 7 presents Pareto diagram related to the main effects of the variables and the interaction of the amount of pesticide absorbed by the Co/Ni/Al-LTH@ZIF-8 composite, results are consistent with the ANOVA results.

The p-value for non-compliance in this design for diazinon removal is < 0.0001, which specifies the suitability of this model. The polynomial that expresses the relationship between the answer and the effective sentences is presented as Eq. (3). where A, B, and C represent the adsorbent dose, pH, and contact time, respectively.

$$R = + 82_{/}30 + 6_{/}08A + 2_{/}10B\text{-}17_{/}87C\text{-}1_{/}54AB + 0_{/}1025AC\text{-}2_{/}16BC\text{-}4_{/}90A^2\text{-}14_{/}24B^2 + 0_{/}1268C^2 \quad (3)$$

The random pattern of residual distribution diagram allows effective uncontrollable factors to be detected during the experiments. The random and two-sidedness distribution of errors in each experiment indicates that the errors are not systematic and the proposed model can be defined to perform defined experiments. Figure. 8a shows the residual curve of each experiment to remove diazinon pesticide by

synthesized adsorbents. As can be seen, the error in performing the experiments is a random error and is not systematic. Therefore, the prepared model is able to provide the percentage of removal of the desired pesticide from the solution. The Predicted R^2 of 0.9874 is in reasonable agreement with the Adjusted R^2 of 0.9967; i.e. the difference is less than 0.2. Also Fig. 8b indicated that the value of adequate precision is 74.789...

3.3. Response Surface

As illustrated in Figure. 9(a-c), the contour and 3D response surface plots were obtained to investigate the interaction between all factors (adsorbent dose, pH and contact time).

Figure 10 presents the values of the desirability and optimal factors affecting the response under different conditions. On the basis of above experiments, removal efficiency of 84% was obtained under following conditions: adsorbent dosage 25 mg, pH value 6.9 and contact time 12 min, which is very close to the actual value.

On the basis of the above results it can be concluded that one of the main factors influenced on the adsorption efficiency is the pH of the solution. As can be observed the pH of 7 of the efficiency adsorption reaches the maximum amount. The zpc value of Co/Ni/Al-LTH@ZIF-8 is about 10 that means at the pH > 10 its surface is *positively* charged, on the other hand, the pK_a of the diazinon is 2.6 [36] indicating that the pH value higher 2.6 of the solution it has *negative* form. Consequently, it can be visualized that *electrostatic attraction* between the Co/Ni/Al-LTH@ZIF-8 and diazinon is one of the main effect for the adsorption process.

In addition, the π–π stacking interaction between the imidazole ring of ZIF-8 and the aromatic ring of organophosphate pesticide could be possible another reasons for the uptake and removal of diazinon by the nanocomposite. Moreover, the possible interaction between zinc metal in the ZIF-8 structure as Lewis acid and sulfur site of diazinon as Lewis base can influence on the adsorption process.

Results indicated that the removal efficiency increases with increasing dose of absorbent, since, the available sites are enhanced by increasing dosage of adsorbent. Contact time also is another factor that can influence on the response, obviously by increasing contact time the removal percent is increased however, after a given time it has no impact. In this experiment, the optimized values of adsorbent dosage, pH and contact time were obtained 24.85 mgr, 6.95 and 11.88 min.

3.4. Study of removal efficiency at optimal levels

The removal of diazinon with an initial concentration (20 ppm) was performed by ZIF-8 and Co/Ni/Al-LTH@ZIF-8 composites. UV-vis spectrum of diazinon solution before removal is shown in Fig. 11(a). The spectra of the diazinon solution after removal by Co/Ni/Al-LTH, ZIF-8 nanoparticles and Co/Ni/Al-LTH@ZIF-8 composite are presented in Fig. 11 (b) and 10 (c) respectively. Obviously, the intensity of the bands are reduced after adsorption process by the above adsorbates. Results revealed that the removal efficiency of the Co/Ni/Al-LTH@ZIF-8 (84%) is more than that of ZIF-8 (68%).

Table 5 presents the comparison between the maximum adsorption capacity (qm) of diazinon onto the Co/Ni/Al-LTH@ZIF-8 nanocomposite and those of other compounds. In following, the results of the comparison between the maximum adsorption capacity (qm) of DIZ by the composite synthesized in this work and other adsorbents are shown in Table 4 Based on the obtained data, it can be stated that the adsorption of DIZ pesticide by Co/Ni/Al-LDH@ZIF-8 composite is a multilayer adsorption method and is consistent with the Freundlich model.

Table 5
Comparison of the maximum adsorption capacity of diazinon onto Co/Ni/Al-LTH@ZIF-8 nanocomposite with other adsorbents.

Adsorbent	q_m (mg g^{-1})	Ref.
MCM-41	25.60	[38]
LOESS	24.69	[39]
Kaolin	48.60	[40]
Iron modified montmorillonite	58.80	[41]
ATZ	15.43	[42]
MZ	61.73	[42]
Co/Ni/Al-LDH@ZIF-8	84	This Work

3.5. Regeneration studies

The reusability of Co/Ni/Al-LDH@ZIF-8 composite in the removal of diazinon under optimal conditions was investigated for four successive cycles and results are presented in Fig. 12. As can be seen, the adsorption efficiency did not decrease significantly after four consecutive uses and the reduction was partial. The results showed that the removal efficiency of diazinon decreased from 84% in the first cycle to 75% in the fourth cycle. The synthesized adsorbent has a good recyclability and reuse.

4. Conclusions

In brief, triple layer hydroxide (Co/Ni/Al-LDH) and Zif-8 imidazolate zeolite frameworks were synthesized by conventional hydrothermal method. In the next step, nanoparticles of ZIF-8 was successfully loaded on the surface of Co/Ni/Al-LTH. The Box – Behnken Design (BBD) method and response surface methodology (RSM) were used to optimize the levels of variables in this study (adsorbent, contact time and pH of the solution). The removal efficiency of Co/Ni/Al-LTH@ZIF-8 (84%) is considerably more than that Co/Ni/Al-LTH and ZIF-8 .

The Co/Ni/Al-LTH@ZIF-8 nanohybrid was satisfactorily used for removal of diazinon in environmental contaminant under optimal conditions. UV-vis spectrophotometry was applied for all measurements. In

fact, Co/Ni/Al-LTH@ZIF-8 nanohybrid surface serves as efficient adsorbent, promoting the removal of diazinon from the wastewater.

References

1. L.P.F. Benício, F.G. Pinto, J. Tronto (2020). Layered double hydroxide nanocomposites for agricultural applications. Layered Double Hydroxide Polymer Nanocomposites (pp. 715–741). Woodhead Publishing
2. J. Cornejo, R. Celis, L. Cox, M. Hermosin, Pesticide-clay interactions and formulations, in *Clay Surfaces: Fundamentals and Applications, Interface Science and Technology*, ed. by F. Wypych, K. atyanarayana (Elselvier Academic Press, Anmsterdam, 2004), pp. 247–266
3. G. Lagaly, Pesticide-clay interactions and formulations. Appl. Clay Sci. **18**, 205–209 (2001)
4. M. Chowdhury, A. Zaman, S. Banik, B. Uddin, M. Moniruzzaman, N. Karim, S.H. Gan, Organophosphorus and carbamate pesticide residues detected in water samples collected from paddy and vegetable fields of the Savar and Dhamrai Upazilas in Bangladesh. Int. J. Environ. Res. Public Health **9**(9), 3318–3329 (2012)
5. G.L. Berg, C. Sine, R.T. Meister, J. Poplyk, *Farm chemicals handbook* (*Meister Publishing Company*, *Willoughby, OH*, 1986)
6. S.J. Garfitt, K. Jones, H.J. Mason, J. Cocker, Exposure to the organophosphate diazinon: data from a human volunteer study with oral and dermal doses. Toxicol. Lett. **134**(1–3), 105–113 (2002)
7. M.E. Báez, J. Espinoza, E. Fuentes, Degradation kinetics of chlorpyrifos and diazinon in volcanic and non-volcanic soils: influence of cyclodextrins. Environ. Sci. Pollut. Res. **25**(25), 25020–25035 (2018)
8. G. Hosseini, A. Maleki, H. Daraei, E. Faez, Y.D. Shahamat, Electrochemical process for diazinon removal from aqueous media: design of experiments, optimization, and DLLME-GC-FID method for diazinon determination. Arab. J. Sci. Eng. **40**(11), 3041–3046 (2015)
9. A. Maleki, F. Moradi, B. Shahmoradi, R. Rezaee, S.M. Lee, The photocatalytic removal of diazinon from aqueous solutions using tungsten oxide doped zinc oxide nanoparticles immobilized on glass substrate. J. Mol. Liq. **297**, 111918 (2020)
10. M. Cycoń, A. Żmijowska, M. Wójcik, Z. Piotrowska-Seget, Biodegradation and bioremediation potential of diazinon-degrading Serratia marcescens to remove other organophosphorus pesticides from soils. J. Environ. Manage. **117**, 7–16 (2013)
11. H. Esfandian, A. Samadi-Maybodi, M. Parvini, B. Khoshandam, Development of a novel method for the removal of diazinon pesticide from aqueous solution and modeling by artificial neural networks (ANN). J. Ind. Eng. Chem. **35**, 295–308 (2016)
12. G. Moussavi, H. Hosseini, A. Alahabadi, The investigation of diazinon pesticide removal from contaminated water by adsorption onto NH4Cl-induced activated carbon. Chem. Eng. J. **214**, 172–179 (2013)

13. M.H. Dehghani, S. Kamalian, M. Shayeghi, M. Yousefi, Z. Heidarinejad, S. Agarwal, V.K. Gupta, High-performance removal of diazinon pesticide from water using multi-walled carbon nanotubes. Microchem. J. **145**, 486–491 (2019)
14. M. Nikou, A. Samadi-Maybodi, K. Yasrebi, E. Sedighi-Pashaki, *Simultaneous monitoring of the adsorption process of two organophosphorus pesticides by employing GO/ZIF-8 composite as an adsorbent*, 23 (Environmental Technology & Innovation, 2021), p. 101590
15. H. Esfandian, A. Samadi-Maybodi, B. Khoshandam, M. Parvini, Experimental and CFD modeling of diazinon pesticide removal using fixed bed column with Cu-modified zeolite nanoparticle. J. Taiwan Inst. Chem. Eng. **75**, 164–173 (2017)
16. A. Samadi-Maybodi, A. Rahmati, Dual metal zeolitic imidazolate frameworks as an organometallic polymer for effective adsorption of chlorpyrifos in aqueous solution. Environ. Eng. Res. **25**(6), 847–853 (2020)
17. S. Tang, H.K. Lee, Application of dissolvable layered double hydroxides as sorbent in dispersive solid-phase extraction and extraction by co-precipitation for the determination of aromatic acid anions. Anal. Chem. **85**(15), 7426–7433 (2013)
18. K.R. Ramakrishna, T. Viraraghavan, Dye removal using low cost adsorbents. Water Sci. Technol. **36**(2–3), 189–196 (1997)
19. X. Xu, J. Zou, X.R. Zhao, X.Y. Jiang, F.P. Jiao, J.G. Yu, … J. Teng, Facile assembly of three-dimensional cylindrical egg white embedded graphene oxide composite with good reusability for aqueous adsorption of rare earth elements. Colloids Surf., A **570**, 127–140 (2019)
20. Y.Q. Tian et al., The silica-like extended polymorphism of cobalt(II) imidazolate three-dimensional frameworks: X-ray single-crystal structures and magnetic properties. Chem—Eur J. **9**(22), 5673–5685 (2003)
21. K.S. Park, Z. Ni, A.P. Côté, J.Y. Choi, R. Huang, F.J. Uribe-Romo, … O.M. Yaghi (2006). Exceptional chemical and thermal stability of zeolitic imidazolate frameworks. Proceedings of the National Academy of Sciences, 103(27), 10186–10191
22. A. Ahmed, M. Forster, J. Jin, P. Myers, H. Zhang, Tuning morphology of nanostructured ZIF-8 on silica microspheres and applications in liquid chromatography and dye degradation. ACS Appl. Mater. Interfaces **7**(32), 18054–18063 (2015)
23. M. Gomar, S. Yeganegi, Adsorption of 5-fluorouracil, hydroxyurea and mercaptopurine drugs on zeolitic imidazolate frameworks (ZIF-7, ZIF-8 and ZIF-9). Microporous Mesoporous Mater. **252**, 167–172 (2017)
24. J. Cravillon, R. Nayuk, S. Springer, A. Feldhoff, K. Huber, M. Wiebcke, Controlling zeolitic imidazolate framework nano-and microcrystal formation: insight into crystal growth by time-resolved in situ static light scattering. Chem. Mater. **23**(8), 2130–2141 (2011)
25. T.A. Saleh, V.K. Gupta, Processing methods, characteristics and adsorption behavior of tire derived carbons: a review. Adv. Colloid Interface Sci. **211**, 93–101 (2014)

26. J. Liu, J. Song, H. Xiao, L. Zhang, Y. Qin, D. Liu, … N. Du, Synthesis and thermal properties of ZnAl layered double hydroxide by urea hydrolysis. Powder Technol. **253**, 41–45 (2014)
27. Y. Pan, Y. Liu, G. Zeng, L. Zhao, Z. Lai, Rapid synthesis of zeolitic imidazolate framework-8 (ZIF-8) nanocrystals in an aqueous system. Chem. Commun. **47**(7), 2071–2073 (2011)
28. J.J. Beh, J.K. Lim, E.P. Ng, B.S. Ooi, Synthesis and size control of zeolitic imidazolate framework-8 (ZIF-8): From the perspective of reaction kinetics and thermodynamics of nucleation. Mater. Chem. Phys. **216**, 393–401 (2018)
29. L. Xu, Y.S. Ding, C.H. Chen, L. Zhao, C. Rimkus, R. Joesten, S.L. Suib, 3D flowerlike α-nickel hydroxide with enhanced electrochemical activity synthesized by microwave-assisted hydrothermal method. Chem. Mater. **20**(1), 308–316 (2008)
30. G.X. Tong, F.T. Liu, W.H. Wu, J.P. Shen, X. Hu, Y. Liang, Polymorphous α-and β-Ni (OH) 2 complex architectures: morphological and phasal evolution mechanisms and enhanced catalytic activity as non-enzymatic glucose sensors. CrystEngComm **14**(18), 5963–5973 (2012)
31. J. Abdi, M. Vossoughi, N.M. Mahmoodi, I. Alemzadeh, Synthesis of metal-organic framework hybrid nanocomposites based on GO and CNT with high adsorption capacity for dye removal. Chem. Eng. J. **326**, 1145–1158 (2017)
32. J. Zhang, J.P. Cheng, M. Li, L. Liu, F. Liu, X.B. Zhang, Flower-like nickel–cobalt binary hydroxides with high specific capacitance: tuning the composition and asymmetric capacitor application. J. Electroanal. Chem. **743**, 38–45 (2015)
33. P.H. Chang, Y.T. Lee, C.H. Peng, Synthesis and Characterization of Hybrid Metal Zeolitic Imidazolate Framework Membrane for Efficient H2/CO2 Gas Separation. Materials **13**(21), 5009 (2020)
34. C.S. Wu, Z.H. Xiong, C. Li, J.M. Zhang, Zeolitic imidazolate metal organic framework ZIF-8 with ultra-high adsorption capacity bound tetracycline in aqueous solution. RSC Adv. **5**(100), 82127–82137 (2015)
35. A. Samadi-Maybodi, M. Nikou, Removal of sarafloxacin from aqueous solution by a magnetized metal-organic framework; Artificial neural network modeling. Polyhedron **179**, 114342 (2020)
36. C. MacBean (ed.), *The pesticide manual: a world compendium* (BCPC, 2012)
37. G. Carja, R. Nakamura, T. Aida, H. Niiyama, Textural properties of layered double hydroxides: effect of magnesium substitution by copper or iron. Microporous Mesoporous Mater. **47**(2–3), 275–284 (2001)
38. M. Armaghan, M.M. Amini, Adsorption of diazinon and fenitothion on MCM-41 and MCM-48 mesoporous silicas from non-polar solvent. Colloid J. **71**(5), 583–588 (2009)
39. K.S. Ryoo, S.Y. Jung, H. Sim, J.H. Choi, Comparative study on adsorptive characteristics of diazinon in water by various adsorbents. Bull. Korean Chem. Soc. **34**(9), 2753–2759 (2013)
40. K. Rida, S. Bouraoui, S. Hadnine, Adsorption of methylene blue from aqueous solution by kaolin and zeolite. Appl. Clay Sci. **83**, 99–105 (2013)

41. P. Kabwadza-Corner, N. Matsue, E. Johan, T. Henmi (2014). Mechanism of Diazinon adsorption on iron modified montmorillonite. American Journal of Analytical Chemistry, 2014
42. H. Esfandian, A. Samadi-Maybodi, M. Parvini, B. Khoshandam, Development of a novel method for the removal of diazinon pesticide from aqueous solution and modeling by artificial neural networks (ANN). J. Ind. Eng. Chem. **35**, 295–308 (2016)

Figures

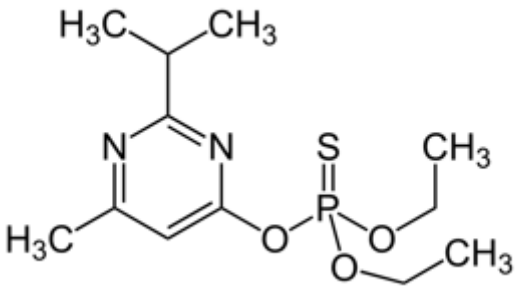

Figure 1

1. Chemical structure of diazinon (Chemical name: O,O-Diethyl O-[4-methyl-6-(propan-2-yl)pyrimidin-2-yl] phosphorothioate)

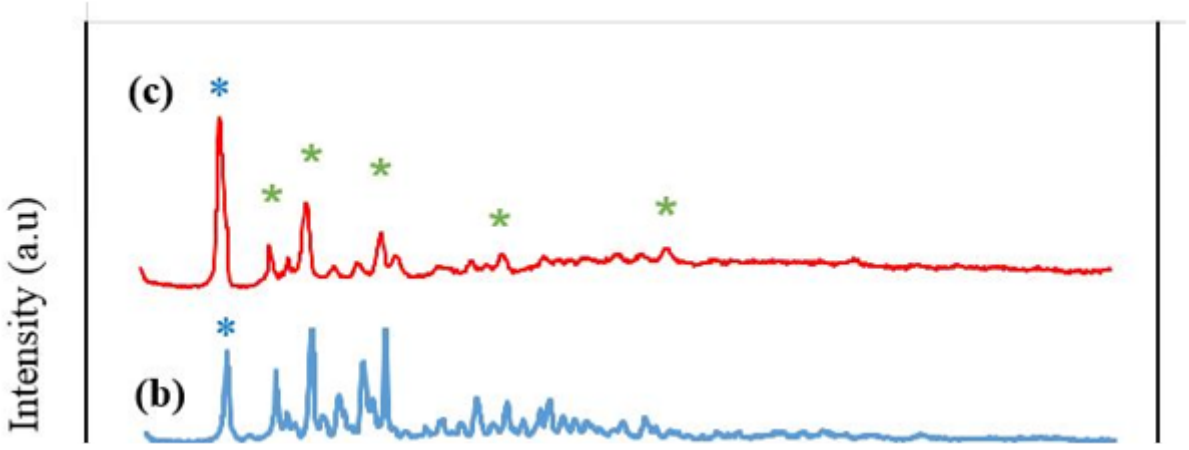

Figure 2

1. XRD patterns for Co/Ni/Al-LTH (a) ,ZIF-8 (b) and Co/Ni/Al-LTH@ZIF-8 (c).

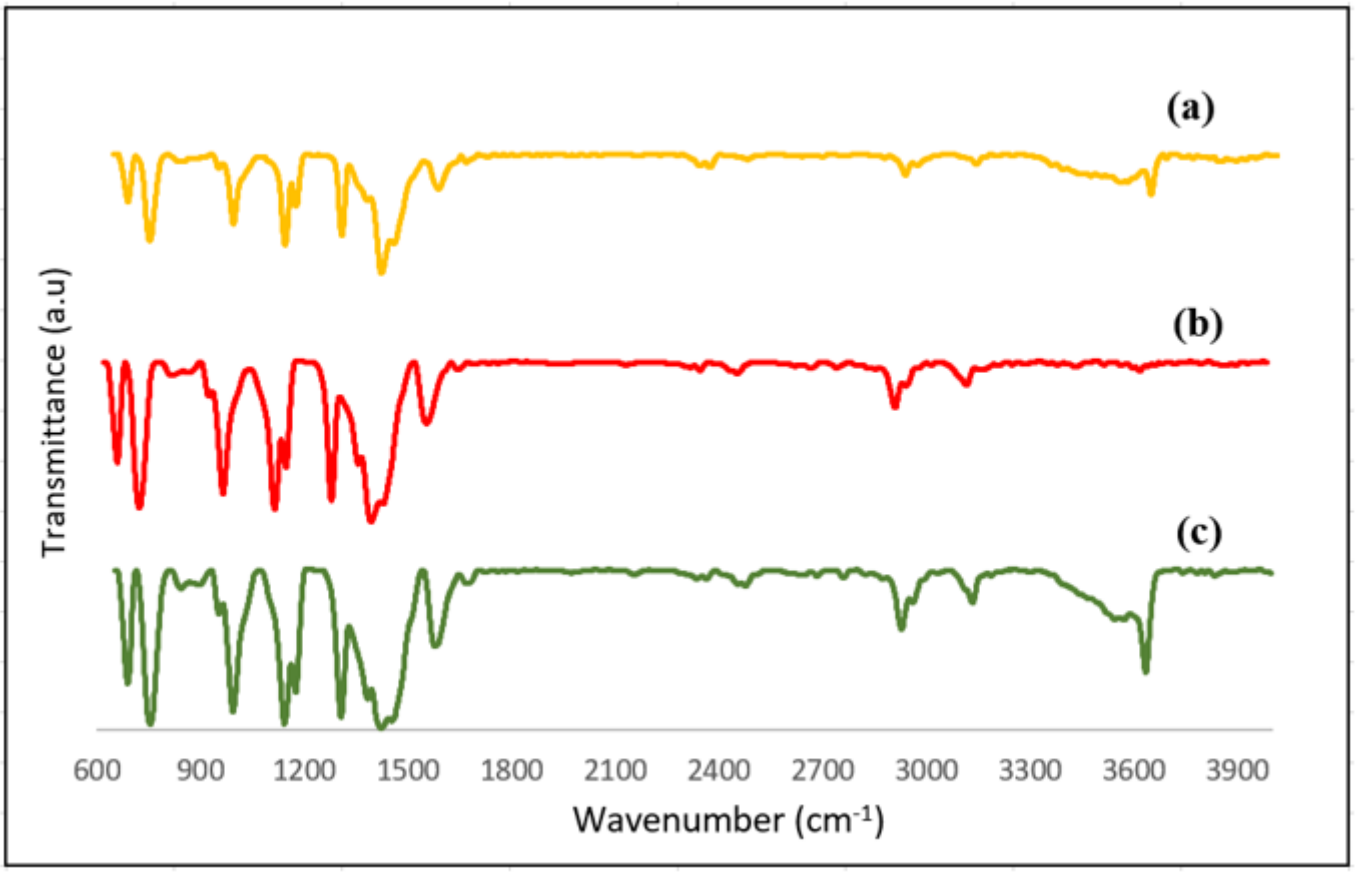

Figure 3

2. FT-IR spectra for Co/Ni/Al-LTH (a), ZIF-8 (b) and Co/Ni/Al-LTH@ZIF-8 (c)

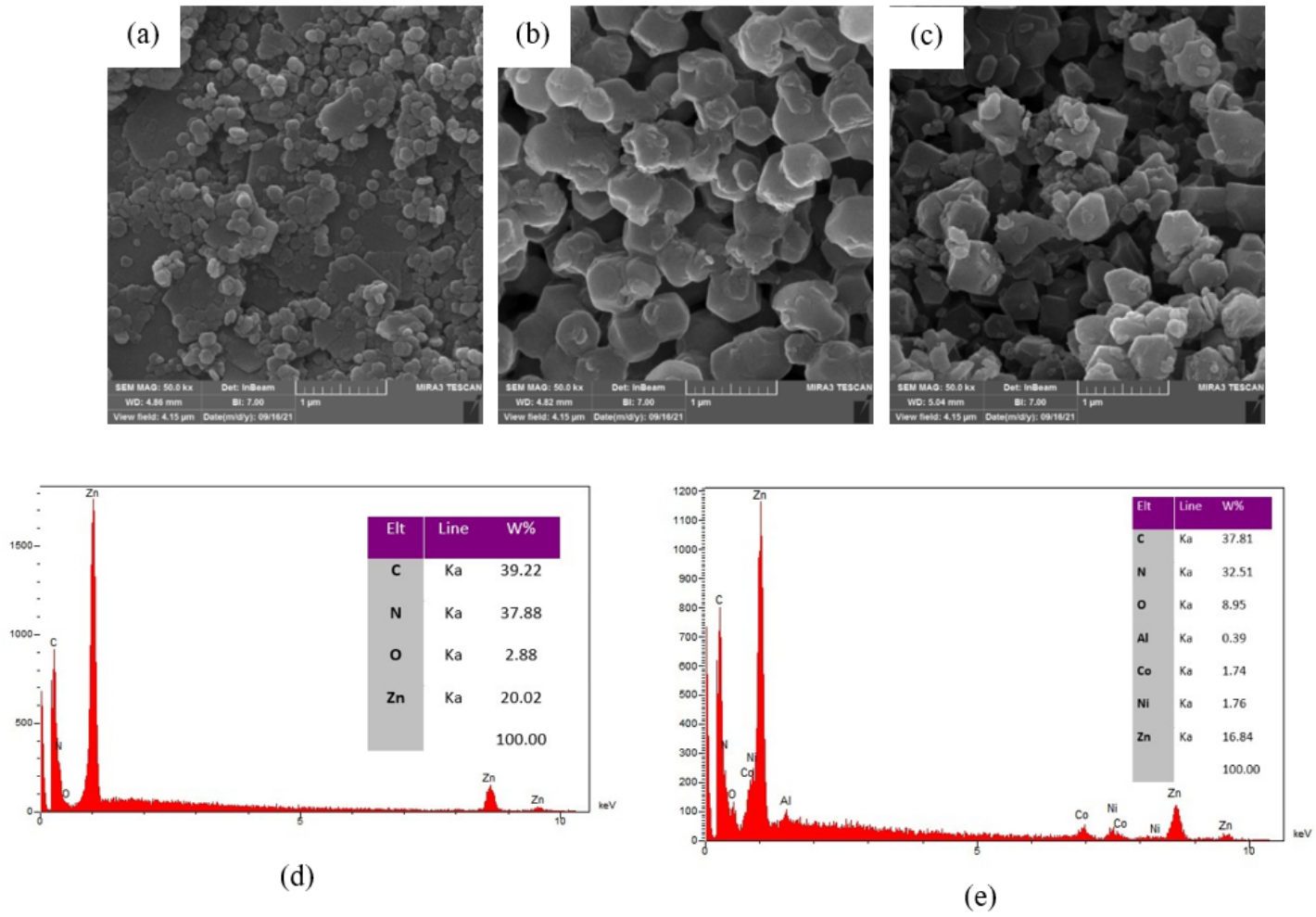

Figure 4

3. FESEM images of the Co/Ni/Al-LTH (a), ZIF-8 (b), Co/Ni/Al-LTH@ZIF-8 (c), EDX spectrum of the ZIF-8 (d) and EDX spectrum of the Co/Ni/Al-LTH @ZIF-8 (e).

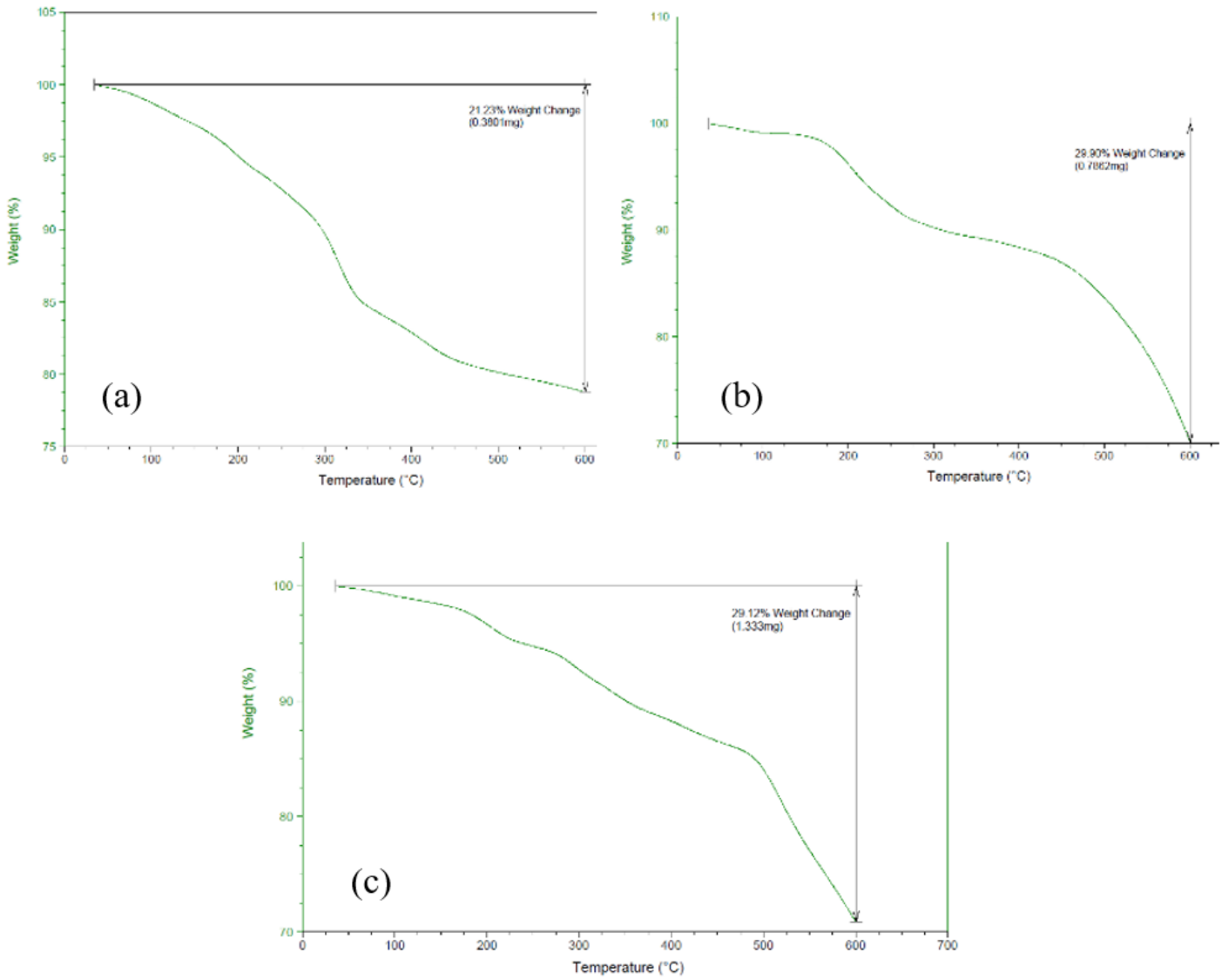

Figure 5

4. Thermogram of Co/Ni/Al-LTH (a), ZIF-8 (b) and Co/Ni/Al-LTH@ZIF-8 composite (c).

Figure 6

5. Zeta potentials of nanocomposite

Figure 7

6. Nitrogen adsorption/desorption (BET) and pore size distribution curves (BJH) of the Co/Ni/Al-LTH (a), ZIF-8 (b) and Co/Ni/Al-LTH@ZIF-8 composite (c).

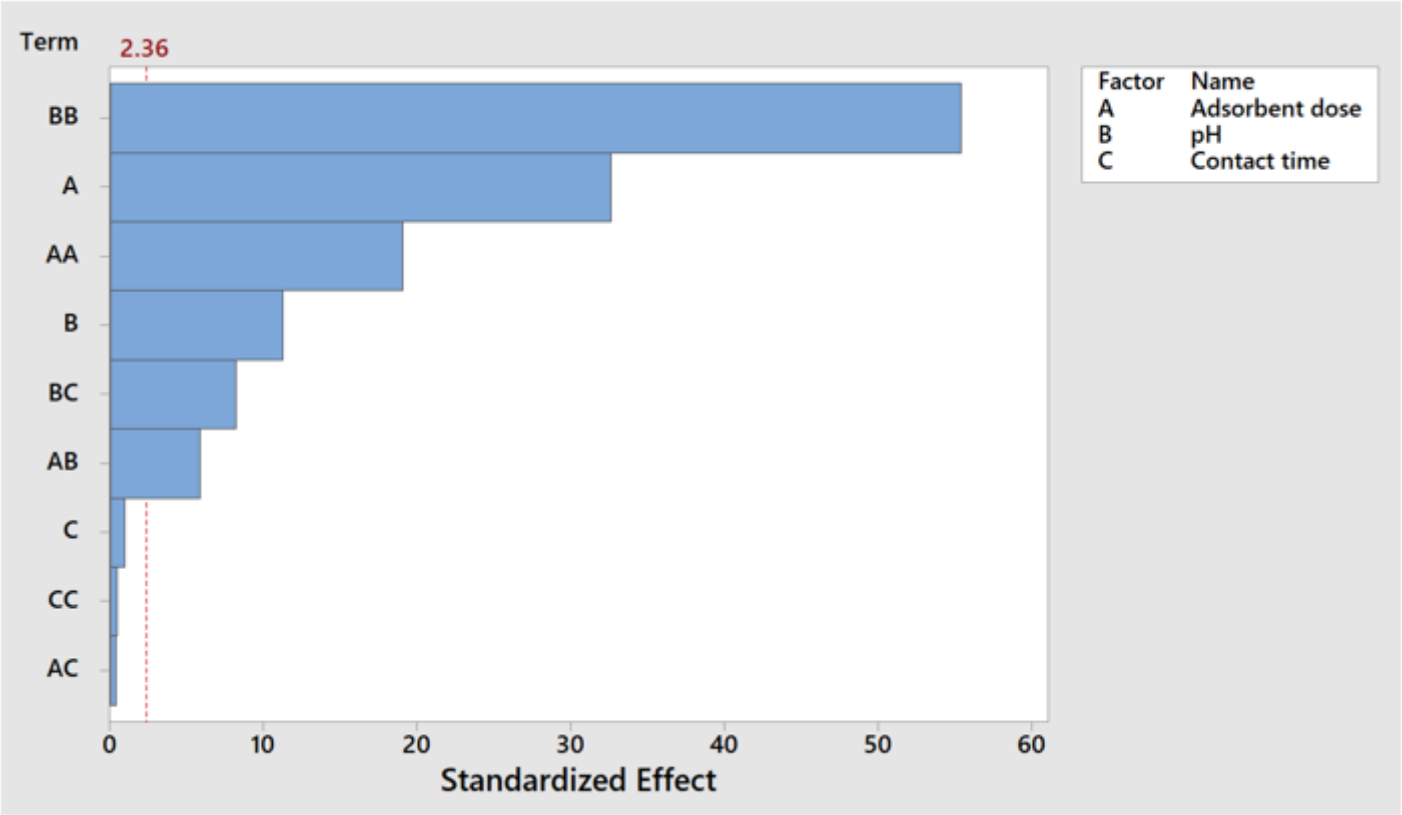

Figure 8

7. Pareto chart of the standardized effects (response is R, α = 0.05)

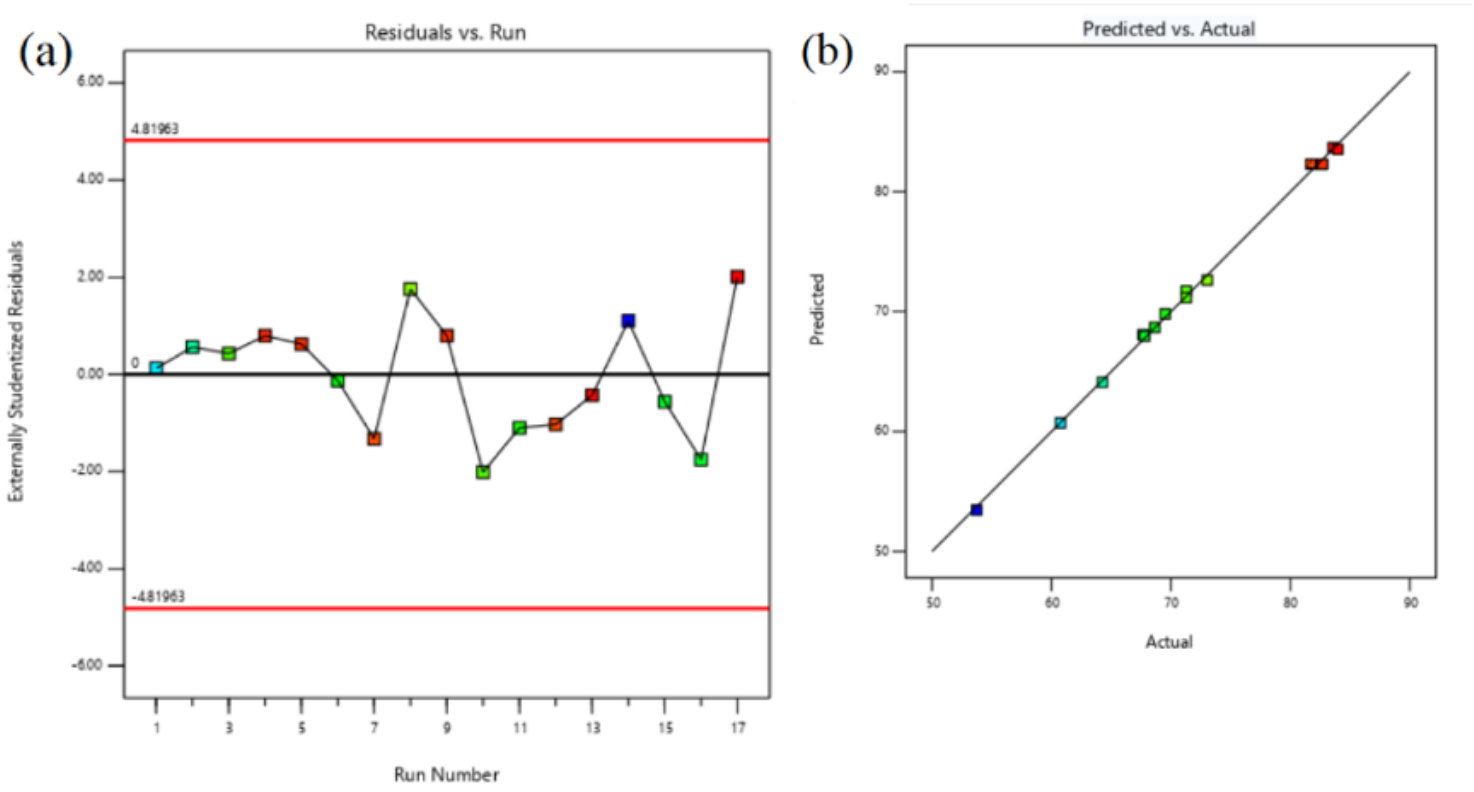

Figure 9

8. Residual distribution curve related to diazinon removal by Co/Ni/Al-LTH@ZIF-8 (a), the fit plot of predicated and experimental responses (b).

Figure 10

9. Contour and 3D response surface plots of the effect of interaction between (a) adsorbent dose (mg) and pH, (b) adsorbent dose (mg) and contact time (min), and (c pH and contact time (min).

Figure 11

10. The values of the desirability and optimal factors affecting the response under different conditions

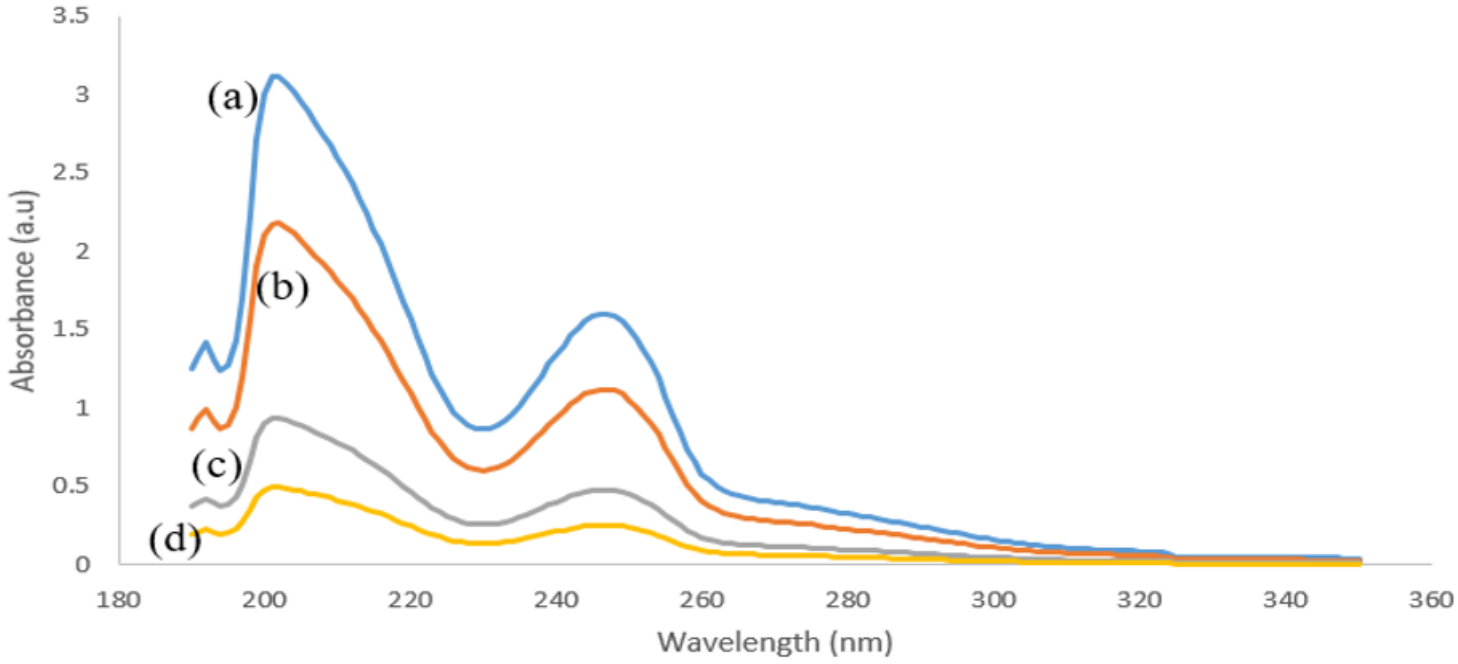

Figure 12

11. UV-Vis spectra of diazinon (a) diazinon solution before adsorption process (20 ppm) (b) after removal by Co/Ni/Al-LTH (c) after removal by ZIF-8 nanoparticles and (d) after removal by Co/Ni/Al-LTH@ZIF-8.

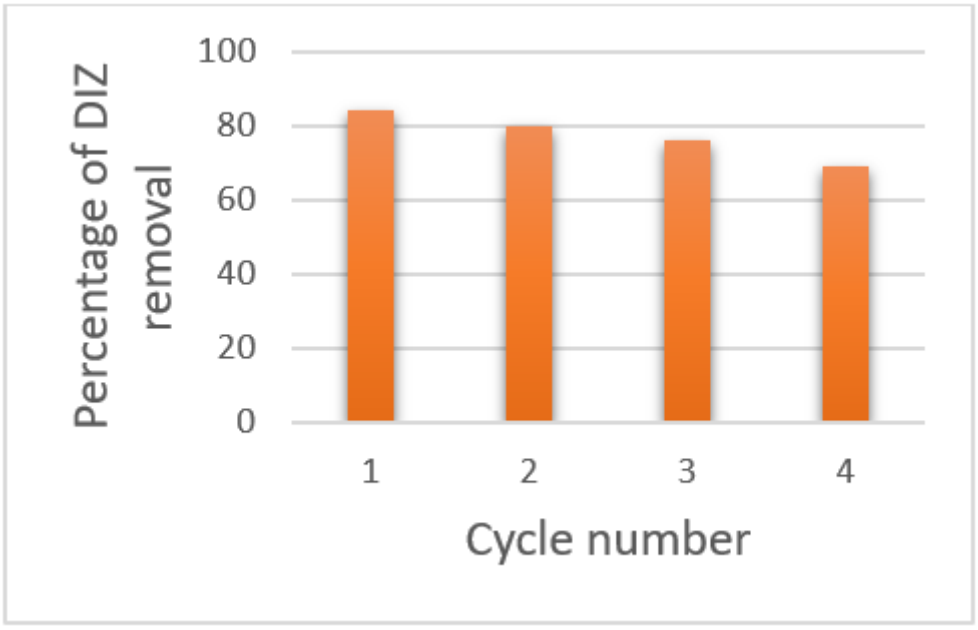

Figure 13

12. The recycle performances of CoNiAl-LTH@ZIF-8.

Supplementary Files

This is a list of supplementary files associated with this preprint. Click to download.

- GRAPHICALABSTRACT.docx